Mechanism of Adenylate Kinase. ^1H, ^{13}C, and ^{15}N NMR Assignments, Secondary Structures, and Substrate Binding Sites†

In-Ja L. Byeon,‡ Honggao Yan,‡,§ Arthur S. Edison,∥ Ed S. Mooberry,∥ Frits Abildgaard,∥ John L. Markley,∥ and Ming-Daw Tsai*,‡

Departments of Chemistry and Biochemistry, The Ohio State University, Columbus, Ohio 43210, and Department of Biochemistry, University of Wisconsin, Madison, Wisconsin 53706

Received August 12, 1993; Revised Manuscript Received September 28, 1993®

ABSTRACT: Backbone ^1H, ^{13}C, and ^{15}N NMR assignments were obtained for the complex of chicken muscle adenylate kinase (AK) with its bisubstrate analog, $MgAP_5A$ [magnesium P^1,P^5-bis(5′-adenosyl)-pentaphosphate]. The assignments were used to elucidate the secondary structures and the enzyme–$MgAP_5A$ interactions. The work involves two unusual features: the molecular weight of AK (21.6 kDa) is one of the largest, on a monomeric basis, for which nearly complete assignment has been reported to date, and the assignment was performed at pH 7.1 instead of the acidic pH used for most other proteins. The results are summarized as follows. Firstly, unambiguous sequential assignments of backbone resonances have been achieved effectively by the combined use of two sequential assignment methods: NOE-directed assignments and the recently developed ^1J-coupling-directed assignments. The starting points of the assignments were provided by several specifically labeled enzyme samples. Over 90% of the backbone ^1H, ^{13}C, and ^{15}N resonances have been assigned. Secondly, spin system information was obtained from the HCCH-TOCSY and HCCH-COSY experiments as well as from 2D homonuclear NMR data. Overall, the side-chain resonances of ca. 40% of the residues, including most of the those displaying NOEs with the adenosine moieties of $MgAP_5A$, have been assigned. Thirdly, secondary structural elements in the AK·$MgAP_5A$ complex were identified by extensive analyses of ^1H–^{15}N 2D HMQC-NOESY and 3D NOESY-HMQC spectra. Overall, the enzyme consists of ca. 60% α-helices and a five-stranded parallel β-sheet. The results are compared with the secondary structure of the free AK from porcine muscle in crystals [Dreusicke, D., Karplus, P. A., & Schulz, G. E. (1988) *J. Mol. Biol. 199*, 359–371]. Lastly, most of the intermolecular NOEs between AK and the adenosine moieties of $MgAP_5A$ have been identified: Thr39, Leu43, Gly64, Leu66, Val67, Val72, and Gln101 are in proximity to the adenosine moiety of the adenosine 5′-monophosphate site, whereas Thr23 is in proximity to that of the adenosine 5′-triphosphate site. These data are discussed in relation to previous results from site-directed mutagenesis, NMR, and X-ray studies and in relation to the mechanism of catalysis.

Adenylate kinase (AK)[1] catalyzes the interconversion reaction between MgATP + AMP and MgADP + ADP. There are five major types of AK: AK1 (from cytosols of mammalian or vertebrate muscles), AKe (from *Escherichia coli*), AKy (from yeast), AK2 (from the mammalian mitochondrial intermembrane space), and AK3 (from the mammalian mitochondrial matrix, specific to GTP instead of ATP). Crystal structures of free porcine muscle AK1 (Dreusicke et al., 1988), $MgAP_5A$ (a bisubstrate analog inhibitor)-bound AKy (Egner et al., 1987) and AKe (Müller & Schulz, 1992), and AMP-bound AK3 (Diederichs & Schulz, 1991) have been determined. However, no crystal structures of AK1 complexed to substrates or inhibitors are available, presumably because such crystals could not be successfully obtained. The substrate sites of AK1 cannot be readily deduced from the complexes of other types of AK since there is a major structural difference between AK1 and other types of AK: AK1 lacks a 30-residue insertion segment which surrounds the adenosine moiety at the MgATP site (Egner et al., 1987; Müller & Schulz, 1992). Thus, although the available crystal structures and site-directed mutagenesis studies have led to a good understanding of the substrate sites of AK, as reviewed by Tsai and Yan (1991), the structure of an AK1 complex with substrates or inhibitors is an important piece of information that remains missing.

† This work was supported by National Institutes of Health Grant GM43268 to M.-D.T. This study made use of a Bruker AM-500 NMR spectrometer at The Ohio State University funded by NIH Grant RR01458 and of the National Magnetic Resonance Facility (Madison, WI) supported by NIH Grants RR02301 and RR02781 and NSF Grant DMB-8415048. This is part 15 in the series, Mechanism of Adenylate Kinase. For part 14, see Shi et al. (1993).

* Address correspondence to this author at the Department of Chemistry, The Ohio State University, 120 W. 18th Ave., Columbus, OH 43210.

‡ The Ohio State University.

§ A former member of the Ohio State Biochemistry Program. Current address: Department of Biochemistry, Michigan State University, East Lansing, MI 48824.

∥ University of Wisconsin.

® Abstract published in *Advance ACS Abstracts*, November 1, 1993.

[1] Abbreviations: ADP, adenosine 5′-diphosphate; AK, adenylate kinase; AMP, adenosine 5′-monophosphate; AP_5A, P^1,P^5-bis(5′-adenosyl)-pentaphosphate; ATP, adenosine 5′-triphosphate; COSY, correlated spectroscopy; DTT, dithiothreitol; EDTA, ethylenediaminetetraacetate; GARP, globally optimized alternating phase rectangular pulse; HCCH-COSY, 3D ^1H–^{13}C–^{13}C–^1H correlation spectroscopy via J_{CC} couplings; HCCH-TOCSY, 3D ^1H–^{13}C–^{13}C–^1H total correlation spectroscopy via isotopic mixing of ^{13}C magnetization; HMQC, heteronuclear multiple quantum coherence; HNCA, amide proton to nitrogen to α-carbon correlation; HN(CA)HA, amide proton to nitrogen to α-proton (via α-carbon) correlation; HNCO, amide proton to nitrogen to carbonyl carbon correlation; HN(CO)CA, amide proton to nitrogen to α-carbon (via carbonyl) correlation; HSMQC, heteronuclear single and multiple quantum coherence; NMR, nuclear magnetic resonance; NOE, nuclear Overhauser effect; NOESY, nuclear Overhauser enhanced spectroscopy; TOCSY, total correlated spectroscopy; TPPI, time-proportional phase incrementation; WT, wild-type; 2D, two-dimensional; 3D, three-dimensional.

0006-2960/93/0432-12508$04.00/0

Table I: Parameters for the NMR Experiments on AK

experiment	nucleus (dimension)	carrier (ppm)	spectral width (ppm)	size (points)[a]
COSY[b]	^{1}H (1)	4.7	16.0	512 (r)
	^{1}H (2)	4.7	16.0	4096 (r)
NOESY[c]	^{1}H (1)	4.7	16.0	512 (r)
	^{1}H (2)	4.7	16.0	4096 (r)
TOCSY[d]	^{1}H (1)	4.7	16.0	384 (r)
	^{1}H (2)	4.7	16.0	4096 (r)
^{15}N HMQC[e] (HSMQC[f])	^{15}N (1)	120.6 (121.1)	28.4 (32.9)	512 (256) (r)
	^{1}H (2)	4.7 (4.7)	13.3 (13.3)	1024 (2048) (r)
^{15}N NOESY-HMQC[g]	^{1}H (1)	4.7[h]	12.3	512 (r)
	^{15}N (2)	120.6	56.7	32 (c)
	^{1}H (3)	8.0	6.7	512 (r)
^{15}N TOCSY-HMQC[g]	^{1}H (1)	4.7	13.3	512 (r)
	^{15}N (2)	121.7	40.1	32 (c)
	^{1}H (3)	4.7	13.3	512 (r)
HNCO[i]	^{15}N (1)	119.2	39.9	32 (c)
	^{13}C′ (2)	176.5	20.1	64 (c)
	^{1}H^N (3)	8.0	6.7	512 (r)
HNCA[i]	^{15}N (1)	119.2	39.9	32 (c)
	^{13}C$^\alpha$ (2)	54.9[j]	33.1	64 (c)
	^{1}H^N (3)	8.0	6.7	512 (r)
HN(CO)CA[k]	^{15}N (1)	119.2	39.9	32 (c)
	^{13}C$^\alpha$ (2)	54.6	33.1	64 (c)
	^{1}H^N (3)	8.0	6.7	512 (r)
HN(CA)HA[l]	^{1}H (1)	4.7	3.8	64 (c)
	^{15}N (2)	119.2	39.9	32 (c)
	^{1}H (3)	4.7	13.3	1024 (r)
HCCH-COSY[m]	^{1}H (1)	2.6	8.0	64 (c)
	^{13}C (2)	40.3	22.1	28 (c)
	^{1}H (3)	2.6	8.0	512 (r)
HCCH-TOCSY[m,n]	^{1}H (1)	2.6	8.0	128 (c)
	^{13}C (2)	40.3	22.1[o]	27 (c)
	^{1}H (3)	2.6	8.0	512 (r)

[a] Real (r) or complex (c) data size. [b] Marion & Wüthrich, 1983. [c] Bodenhausen et al., 1984. [d] Bax & Davis, 1985. [e] Mueller, 1979. [f] Zuiderweg, 1990. [g] Marion et al., 1989a; Clubb et al., 1991. [h] A 45° phase shift was used to move the carrier to the center of the amide region (Marion et al., 1989a). [i] Ikura et al., 1990. [j] The chemical shift is obtained after correction for more resonant effects (McCoy & Müller, 1992). [k] Bax & Ikura, 1991. [l] Clubb et al., 1992. [m] Bax et al., 1990a. [n] Bax et al., 1990b. Extensive folding was used in the ^{13}C dimension. [o] The HCCH-TOCSY spectrum was recorded with a DIPSI-3 (Shaka et al., 1988) mixing sequence and a mixing time of 24.8 ms.

Even if such a crystal structure was available, it is always desirable to have the solution structure since the latter can be directly correlated with the catalytic mechanism of the enzyme.

In this article, we report a major advance toward the solution of the tertiary structure of AK1·MgAP$_5$A in solution, using multiple resonance 2D and 3D NMR techniques: assignment of ≥90% of backbone ^{1}H, ^{15}N, and ^{13}C resonances and ca. 40% of side-chain protons, determination of secondary structures, and identification of NOEs between the two adenosine moieties of AP$_5$A and the active-site residues of AK. Three aspects of this study are particularly noteworthy: The chicken muscle AK1 used in this study (193 amino acids, 21.6 kDa) is one of the largest proteins, on a monomeric mass basis, for which the majority of backbone resonances and a significant portion of side-chain protons have been assigned. Unlike most assignment studies, which have utilized samples at acidic pH to optimize the detection of amide protons, our investigations were conducted at a neutral, catalytically relevant pH value (7.1). Most importantly, the NOE cross peaks between AK and AP$_5$A provided useful information on the location of the substrate sites of AK1 in solution.

MATERIALS AND METHODS

AK Purification and NMR Sample Preparation. Recombinant chicken muscle AK was prepared as previously described (Tian et al., 1988). Uniformly labeled enzymes were prepared by growing bacteria in M9 minimal medium with $(^{15}NH_4)_2SO_4$ as the sole nitrogen source or $(^{15}NH_4)_2SO_4$ and [^{13}C$_6$]glucose as the sole nitrogen and carbon sources, respectively. Selectively labeled enzymes were prepared by transforming the AK expression plasmid into a particular *E. coli* strain and growing the bacteria in a defined medium with isotopically enriched amino acids and all other unenriched amino acids to repress endogenous synthesis by the bacteria (Muchmore et al., 1989). The DL39 strain was used for [^{15}N]-Leu/[^{13}C′]Val- and [^{15}N]Val/[^{13}C′]Leu-labeled samples, KBT001 for a [^{15}N]Lys/[^{13}C′]Leu-labeled sample, DL49SPH for a [^{15}N]Gly/[^{15}N]Ser/[^{13}C′]Val-labeled sample, and DL39G for a [^{15}N]Gly-labeled sample. The DL strains were obtained from D. M. LeMaster (Northwestern University) and the KBT strain from J. Adler (University of Wisconsin). The isotopically enriched amino acids, $(^{15}NH_4)_2SO_4$ and [^{13}C$_6$]-glucose were purchased from either Isotec Inc. or Cambridge Isotope Laboratories. Unenriched amino acids were obtained from Sigma.

Samples for NMR typically contained about 2 mM enzyme, 3 mM AP$_5$A, 6 mM $MgCl_2$, 65 mM KCl, 2 mM DTT, and 0.5 mM EDTA in 20 mM perdeuterated Tris buffer and 90% H_2O/10% D_2O or 99.996% D_2O at pH 7.1. DTT was obtained from United States Biochemicals. Perdeuterated Tris and D_2O were purchased from MSD. AP$_5$A, $MgCl_2$, KCl, and EDTA were obtained from Sigma.

NMR Spectroscopy. All NMR experiments were recorded at 34 °C unless otherwise specified. All of the homonuclear COSY (Marion & Wüthrich, 1983), NOESY (Bodenhausen et al., 1984), and TOCSY (Bax & Davis, 1985) and some of the heteronuclear 2D ^{15}N HMQC experiments (Marion et al., 1989a) were conducted on a Bruker AM-500 spectrometer at Ohio State University. The other heteronuclear experiments were recorded on an AM-600 spectrometer at the National Magnetic Resonance Facility (Madison, WI) extensively modified with third and fourth channels (Mooberry et al.,

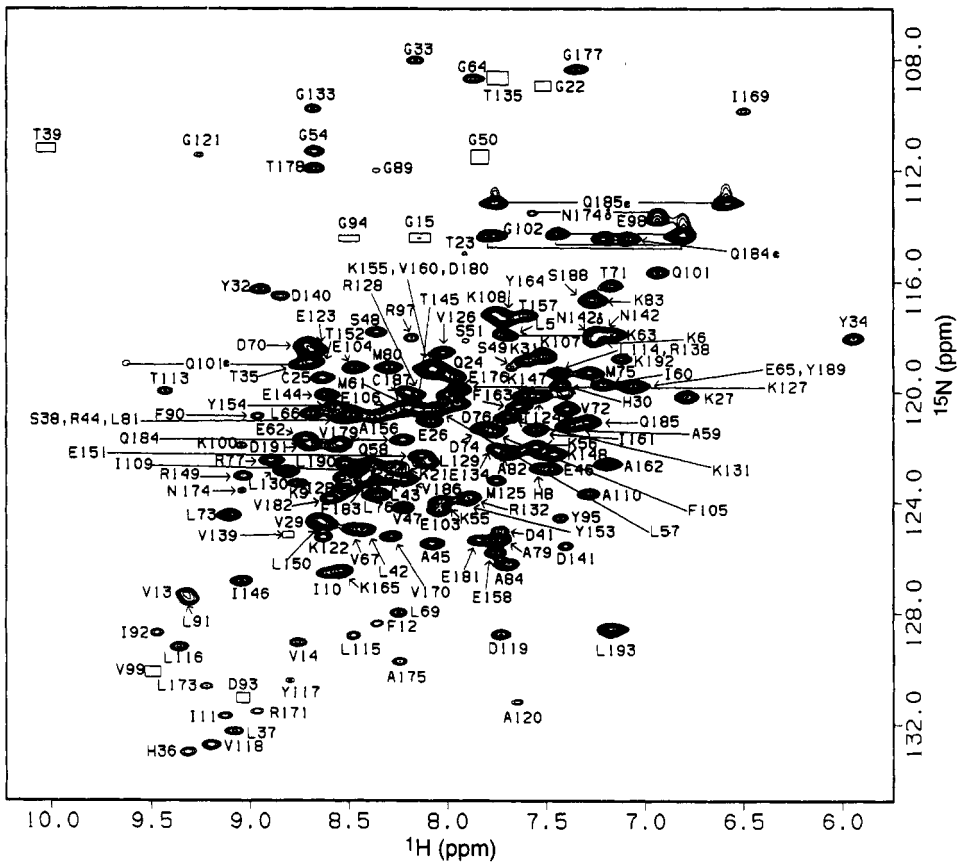

FIGURE 1: Two-dimensional ^{1}H–^{15}N HSMQC spectrum of AK·MgAP$_5$A. The assigned cross peaks are labeled according to the residue number. Weak cross peaks indicated with boxes are clearly observable when lower contour levels are plotted. Horizontal lines connect cross peaks from the NH_2 groups of Asn and Gln.

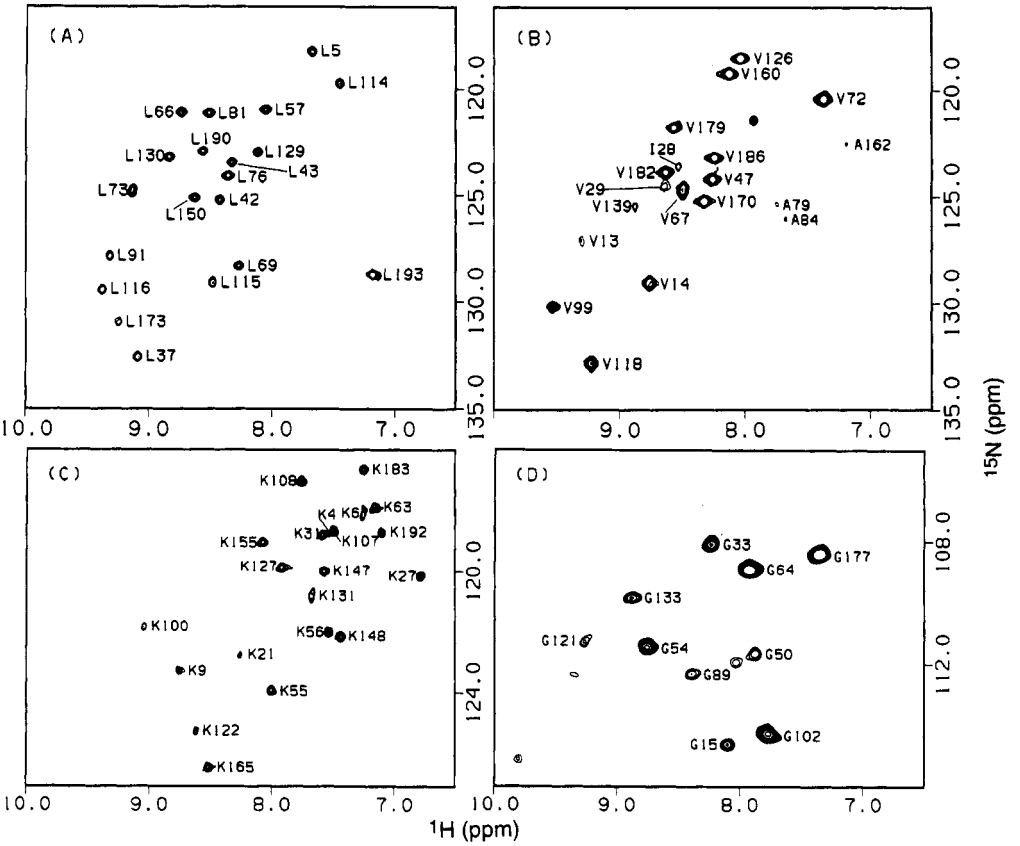

FIGURE 2: HMQC and HMSQC spectra of specifically labeled AK: (A) [^{15}N]Leu/[^{13}C′]Val-labeled, HMQC, at 27 °C; (B) [^{15}N]Val/[^{13}C′]Leu-labeled, HMQC, at 27 °C; (C) [^{15}N]Lys/[^{13}C′]Leu-labeled, HSMQC, at 34 °C; (D) [^{15}N]Gly-labeled, HMQC, at 34 °C.

1992). Three-dimensional NMR data were collected as a series of 2D experiments with four separate automation files to obtain quadrature detection in the third dimension. A Pascal program in Bruker PASCOM (1988 version) was written to

Table II: Assignments for Chicken Muscle Adenylate Kinase at 34 °C and pH 7.1[a]

	^{15}N	H^N	$^{13}C'$	$^{13}C^\alpha$	H^α	H^β	others
S1							
T2							
E3			173.2	57.5(?)			
K4	118.6	7.54	175.9	56.3	4.14		
L5	118.0	7.69	175.9	53.2	4.82		
K6	118.1	7.27		57.1	4.03		
H7			174.0	53.7		2.93, 3.15	H^δ 6.90, H^ϵ 7.88
H8	122.8	7.55	174.9	56.1	4.43		H^δ 6.73, H^ϵ 7.96
K9	123.3	8.77	174.6	55.2	4.41		
I10	126.6	8.63	172.8	59.2	4.54		
I11	131.7	9.14	174.9	57.5	4.75	1.91	H^γ 0.73, 1.22, $H^{\gamma m}$ 0.79, H^δ 0.79
F12	128.4	8.38	174.0	51.8	5.57	2.85, 3.38	H^δ 6.68, H^ϵ 6.54, H^ζ 6.40
V13	127.3	9.35	173.3	60.9	4.94	2.16	H^γ 0.79, 0.90
V14	129.1	8.78	172.5	58.5	4.58	1.82	H^γ 0.77, 0.83
G15	114.4	8.16		43.5			
G16							
P17		–					
G18							
S19							
G20			172.4	43.3(?)			
K21	122.7	8.29		55.7			
G22	108.9	7.45	171.4	44.2			
T23	115.0	7.93	175.8	65.6	3.80	4.24	H^γ 1.06
Q24	119.4	7.98	177.6	56.1	3.99		
C25	119.5	8.66	174.7	63.6	3.97		
E26	121.1	8.10	177.5	58.4	3.89		
K27	120.2	6.79	178.3	57.5	3.80		
I28	123.5	8.55	177.3	64.3	3.76		
V29	124.7	8.67	177.9	66.2	3.50	2.26	H^γ 1.03, 1.24
H30	119.7	7.45	174.8	57.7	4.28	3.14	H^δ 7.03, H^ϵ 7.77
K31	118.9	7.63	175.6	57.0	4.17		
Y32	116.3	8.97	176.5	57.6	4.40	2.52, 2.68	H^δ 7.36, H^ϵ 6.90
G33	108.0	8.17	173.5	44.7	4.02, 3.50		
Y34	118.0	5.94	171.9	55.9	4.44	2.23, 2.93	H^δ 6.62, H^ϵ 6.51
T35	117.4	8.77	180.6(?)	61.0(?)	4.38	3.92	H^γ 1.30
H36	133.0	9.35	172.4	52.4	5.47	2.86, 3.28	H^δ 6.83, H^ϵ 7.99
L37	132.3	9.09		51.1	4.63		
S38	120.9	8.57		52.5			
T39	111.2	10.06				3.90	H^γ 1.18, $O^\gamma H$ 6.20
G40			173.4	45.7			
D41	125.0	7.75	178.4	56.0	4.20		
L42	125.0	8.43	178.7	56.5	4.06		H^γ 1.90, H^δ 0.65, 0.83
L43	123.1	8.31	177.7	56.4	3.83		H^γ 1.79, H^δ 0.24, 0.62
R44	120.9	8.51	177.6	59.1	3.83		
A45	125.5	8.08	179.1	53.3	4.23	1.54	
E46	122.8	7.49	179.2	57.1	4.19		
V47	124.2	8.24	178.4	65.8	3.43	2.38	H^γ 0.92, 1.21
S48	117.8	8.37	173.4	59.4	4.29		
S49	119.1	7.69	174.8	58.9	4.25		
G50	111.5	7.86	172.9	44.1			
S51	118.2	7.93		55.7			
E52							
R53			177.1	57.6	4.65(?)		
G54	111.3	8.70	173.4	45.7	3.45		
K55	124.0	8.05	178.7	58.0	4.11		
K56	122.0	7.57	178.0	57.2	4.18		
L57	120.6	8.07	177.3	55.8	4.07		
Q58	122.6	8.43	175.9	58.0	3.85		
A59	121.2	7.39	178.5	53.0	4.20	1.52	
I60	119.7	7.23	177.2	63.3	3.70		
M61	120.6	8.25	179.8	58.0	4.20		
E62	121.7	8.74	175.0	57.8	3.92		
K63	117.9	7.18	175.5	54.4	4.47		
G64	108.7	7.88	171.8	44.9			
E65	119.8	7.06	173.5	52.9	4.45	2.91	
L66	120.8	8.71	175.8	52.8	4.49		H^γ 1.61, H^δ 0.20, 0.62
V67	125.0	8.51		59.4	4.30	1.91	H^γ 1.05, 1.11
P68		–	174.6(?)	60.7			
L69	128.0	8.24	176.5	58.4	4.19		
D70	118.3	8.74	176.5	56.1	4.20		
T71	116.1	7.18	174.4	64.4	3.96	4.04	H^γ 1.07
V72	120.6	7.42	175.0	64.3	3.55	1.80	H^γ 0.62, 0.99
L73	124.5	9.12	176.8	56.6	4.02		
D74	121.3	7.84	176.9	56.2	4.24		
M75	119.3	7.30	177.9	57.6	4.05		
L76	123.7	8.36	176.0	56.1	3.81		H^γ 1.40, H^δ 0.36, 0.59
R77	122.5	8.91	176.5	58.4	3.50		
D78	120.4	7.97	177.7	56.0	4.32		

Table II (Continued)

	^{15}N	H^N	$^{13}C'$	$^{13}C^\alpha$	H^α	H^β	others
A79	125.3	7.76	178.8	53.2	4.18	1.48	
M80	119.1	8.31	177.4	57.6	3.61		
L81	120.8	8.51	178.6	56.4	3.88		
A82	122.2	7.71	177.8	52.8	4.23	1.57	
K83	116.7	7.27	176.1	52.8	4.01		
A84	126.2	7.70		54.7	3.95	1.62	
D85							
T86							
S87							
K88			175.5	54.5			
G89	112.0	8.37	169.8	43.3	4.01		
F90	120.9	8.98	171.9	56.5	5.27		H^δ 6.99, H^ϵ 6.81, H^ζ 6.95
L91	127.5	9.32	172.87	51.3	4.97	2.09	
I92	128.7	9.50		58.2	4.84	2.43	$H^{\gamma m}$ 0.99
D93	131.0	9.04		50.6(?)	4.95		
G94	114.5	8.55	171.4	44.3			
Y95	124.5	7.44		52.9	4.19	2.78	H^δ 6.58, H^ϵ 6.54
P96		–	175.0	59.7			
R97	118.0	8.19	173.1	52.3	4.33		
E98	113.8	6.94		52.5	4.63		
V99	130.2	9.53	177.5	67.0	3.10	1.79	H^γ 0.12, 0.71
K100	121.9	9.07	177.8	57.5	4.25		
Q101	115.7	6.95	179.9	57.5	4.05		N^ϵ 119.0, H^ϵ 9.64
G102	114.3	7.77	173.3	46.4			
E103	124.3	8.06	178.6	58.5	4.17		
E104	119.1	8.49	177.1	57.3	4.19		
F105	121.4	7.79	175.7	60.4	4.00	3.56, 3.81	H^δ 7.19, H^ϵ 7.22, H^ζ 6.93
E106	120.7	8.30	176.0	57.5	4.12		
K107	118.7	7.52	177.0	57.0	4.08		
K108	117.2	7.78	175.4	56.0	4.22		
I109	122.9	8.37	171.2	61.5	3.82	0.76	$H^{\gamma m}$ 0.41
A110	123.7	7.30		49.5	4.64	1.38	
P111		–					
P112		–	174.5	60.0			
T113	120.0	9.44	173.4	62.8	4.09	3.71	H^γ 1.28
L114	119.3	7.45	171.5(?)	52.0	4.50		
L115	128.8	8.50	173.0	52.9	5.27		
L116	129.2	9.38	170.9(?)	52.0	4.78		
Y117	130.4	8.82	171.9	50.8	5.59	2.67, 2.83	H^δ 6.87, H^ϵ 6.90
V118	132.8	9.22	171.3	60.1	3.68	2.13	H^γ 0.58, 0.71
D119	128.8	7.75	172.4	53.1	4.15		
A120	131.2	7.66	174.4	47.9	4.70	1.09	
G121	111.4	9.28	173.0	43.0	3.96		
K122	125.3	8.64	176.5	59.4	3.96		
E123	118.5	8.73	177.9	58.3	3.96		
T124	120.1	7.56	174.0	64.5	3.72	4.26	H^γ 0.89
M125	123.2	7.78	176.0	60.2	3.40		
V126	118.6	8.06	176.5	66.3	3.34	2.18	H^γ 0.96, 1.06
K127	119.9	7.96	179.0	58.5	3.95		
R128	120.1	8.17	179.1	58.1	3.98		
L129	122.6	8.11	177.6	55.9	4.04		
L130	122.9	8.83	179.3	56.0	4.11		
K131	120.9	7.71	178.0	56.8	4.25		
R132	123.8	7.90	177.9	57.9	4.19		
G133	109.8	8.69	173.4	45.5			
E134	122.1	7.78	176.9	57.3	4.27		
T135	108.8	7.78			4.60	4.41	H^γ 1.27
S136							
G137			171.4	44.6			
R138	119.3	7.44		54.2	4.56		
V139	125.2	8.88	174.5	62.4	4.01	2.24	H^γ 1.03
D140	116.5	8.85	174.9	51.4	4.54		
D141	125.6	7.42	172.9	52.2	4.67		
N142	117.9	7.23		50.6	4.82	2.88, 3.01	N^δ 117.9, H^δ 7.26, 7.71
E143			176.2	60.0	3.77		
E144	120.1	8.66	178.0	58.2	4.16		
T145	120.6	8.15	175.9	65.2	4.00	4.12	H^γ 1.25
I146	126.8	9.05	175.9	65.8	3.48		
K147	120.1	7.61	178.3	59.1	4.00		
K148	122.3	7.47	177.9	57.0	4.27		
R149	123.0	9.05	179.3	58.0	4.10		
L150	124.8	8.63	175.8	57.2	3.98		
E151	122.3	8.15	177.9	58.5	4.26		
T152	118.9	8.71	174.0	64.9	3.95	4.33	H^γ 1.17
Y153	123.9	7.91	175.9	60.2	4.09		
Y154	120.5	8.56	175.9	61.3	3.92		H^δ 7.34, H^ϵ 6.95
K155	119.1	8.11	175.8	57.0	4.23		
A156	120.9	8.40	176.9	51.9	4.52	1.52	

Table II (Continued)

	^{15}N	H^N	$^{13}C'$	$^{13}C^\alpha$	H^α	H^β	others
T157	117.2	7.61	174.0	63.1	3.99	4.03	H^γ 1.12
E158	125.8	7.78		55.7	3.77		
P159		–	176.7	64.5	4.36		
V160	119.2	8.11	175.7	64.1	3.53	2.38	H^γ 0.75, 0.92
I161	121.3	7.56	176.5	61.9	3.48	1.96	H^γ 0.41, 1.05, $H^{\gamma m}$ 0.52, H^δ 0.19
A162	122.6	7.20	178.3	53.4	4.00	1.47	
F163	120.5	7.65	176.1	59.2	4.19	3.01, 3.05	H^δ 6.43, H^ϵ 7.00, H^ζ 7.16
Y164	117.3	7.74	176.9	60.2	4.22	2.54, 2.98	H^δ 7.12, H^ϵ 6.85
K165	126.5	8.56		58.3	4.06		
G166	113.3	6.61	173.4	44.4	3.44(?)		
R167	123.1	8.43		53.9	4.46		
G168			174.8	44.7			
I169	109.9	6.51	173.1	60.1	4.51	2.23	$H^{\gamma m}$ 0.91
V170	125.2	8.30	175.5	61.8	4.52	2.21	
R171	131.5	8.98	172.4(?)	50.7			
Q172	128.5	8.96	173.0	54.9			
L173	130.7	9.24		51.0	4.79		
N174	123.6	9.06	174.6	51.4	4.90	2.89, 3.08	N^δ 111.9, H^δ 6.95, 7.59
A175	129.8	8.25	176.0	50.3	4.45	1.27	
E176	120.1	8.02	175.5	55.6	4.08		
G177	108.4	7.36	171.3	43.0			
T178	111.9	8.69	173.9	60.0	4.78	4.74	H^γ 1.41
V179	121.9	8.56	177.5	65.6	3.44	1.79	H^γ 0.57, 0.69
D180	119.2	8.08	177.5	55.9	4.59		
E181	125.4	7.88	179.2	57.8	4.04		
V182	123.9	8.61	177.2	64.9	3.77	2.23	H^γ 1.01, 1.08
F183	123.1	8.45	177.0	59.3	4.72		H^δ 7.57, H^ϵ 7.15, H^ζ 7.00
Q184	121.7	8.25	178.0	57.9	3.85		H^γ 2.33, 2.47, N^ϵ 112.8, H^ϵ 7.10, 7.22
Q185	121.1	7.28	177.2	57.1	3.93		H^γ 2.22, 2.33, N^ϵ 111.5, H^ϵ 6.51, 7.78
V186	123.2	8.24	177.1	66.0	3.43	2.64	H^γ 1.01, 1.26
C187	120.0	8.25	174.5	61.3	4.13		
S188	116.6	7.29	175.0	59.7	4.22		
Y189	119.8	7.08	177.7	56.7	4.82		H^δ 7.02, H^ϵ 6.74
L190	122.6	8.54	178.1	55.7	4.00		
D191	121.9	8.71	175.7	55.1	4.00		
K192	118.8	7.13	174.6	53.8	4.47		
L193	128.6	7.18		55.3	4.15	1.65	

[a] Proton chemical shifts are ±0.01 ppm. The nitrogen and carbon chemical shifts are ±0.1 ppm. Question marks indicate that the assignments are uncertain or tentative. Dashes indicate that there is no NH proton in proline.

generate a master executable file, which started the four automation files with the appropriate dwell times and initial delays. In order to eliminate the spectrometer dead time, the indirectly detected dimension of the 2D planes was always collected with a timer box available from Tschudin Associates (Kensington, MD). Heteronuclear decoupling was generated with a GARP box from Tschudin Associates. When possible, the initial delays in all indirectly detected dimensions were adjusted to give 180° first-order and 90° zero-order phase corrections (Bax et al., 1991). Quadrature in the indirectly observed dimensions was obtained with States-TPPI (Marion et al., 1989b) for all experiments except the 2D ^{15}N HMQC (or HSMQC) and 3D ^{15}N NOESY-HMQC, where TPPI (Drobny et al., 1979) was employed. Quadrature in the directly detected dimension was with Bruker sequential acquisition. The experiments, spectral parameters, and original references are summarized in Table I. The mixing time used in all NOESY experiments was 0.12 s. Our previous study indicated that spin diffusions are minimal under this condition (Shi et al., 1993).

All data were processed with Felix (ver. 2.05, Hare Research, Inc.) installed on Silicon Graphics Indigo computers. Most of the indirectly detected dimensions of the data shown in Table I were first extended by 25–50% by linear prediction, multiplied by a squared cosine function, and zero-filled one time before Fourier transformation. After the indirectly detected dimensions were processed, the acquisition dimension was inverse Fourier transformed and the first point was corrected by linear prediction (Marion & Bax, 1989). Apodization by a squared cosine function was applied followed by Fourier transformation. Due to the dispersive signal in the (non-constant time) HCCH-COSY experiment (Bax et al., 1990a), the carbon dimension was multiplied by a squared sine function shifted by 50°.

Proton chemical shifts were referenced to internal sodium 3-(trimethylsilyl)propionate-*2,2,3,3-d*$_4$ at 0.00 ppm. Nitrogen chemical shifts were referenced to external $^{15}NH_4Cl$ (2.9 M) in 1 M HCl at 24.93 ppm (Stockman et al., 1992). The carbon chemical shifts were referenced to external 5% dioxane at 67.8 ppm.

RESULTS

General Conditions. There are three important features in our NMR experiments: Although AK has a high molecular weight on the NMR standard (21.6 kDa for the free enzyme, 22.5 kDa for the complex), it produces proton NMR spectra with relatively narrow line widths. This is possibly a consequence of the lack of protein aggregation, lack of disulfide bonds, and the conformational flexibility of AK (Dahnke & Tsai, 1993). Secondly, although most total assignments of proteins have been performed at acidic pH so as to maximize the resolution of H^N resonances, the present work was conducted at neutral pH (7.1). This allows direct correlation between structural properties and catalysis. Lastly, although AP_5A is a symmetrical molecule, the free and bound forms are in slow exchange on the NMR time scale. This allows the identification of NOEs between the active-site residues and the MgATP and AMP moieties of AP_5A. This feature is critically important in mapping out the two substrate sites.

Strategy for Sequential Assignments. (A) Homonuclear 2D NMR. Many side-chain spin systems of Ala, Thr, Val,

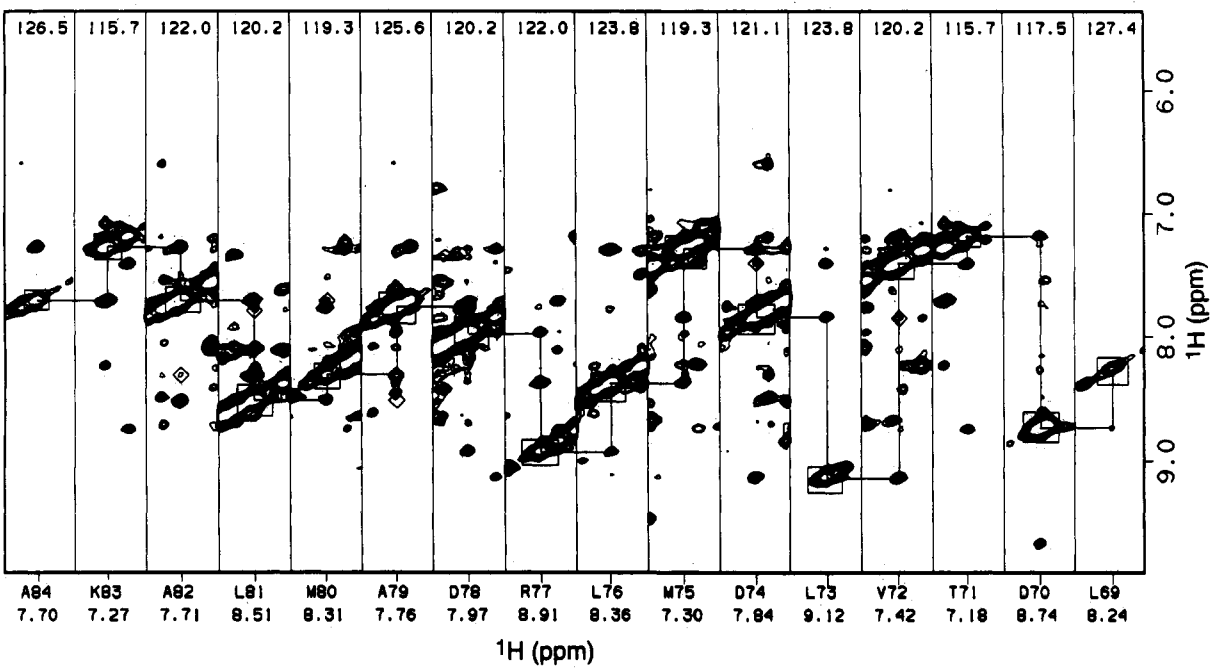

FIGURE 3: Sequential assignments for the Ala84–Leu69 peptide stretch from $d_{NN(i,i+1)}$ NOE connectivities found in the 3D ^{15}N NOESY-HMQC data (t_{mix} = 0.12 s). Slices were taken at the specific ^{15}N chemical shifts shown at the top of each panel. Residue number assignments and amide proton chemical shifts are indicated below each panel. The H^N diagonal peaks are boxed, the sequential $d_{NN(i,i+1)}$ NOE connectivities are indicated by lines, and the $d_{NN(i,i+2)}$ NOEs are indicated by diamonds.

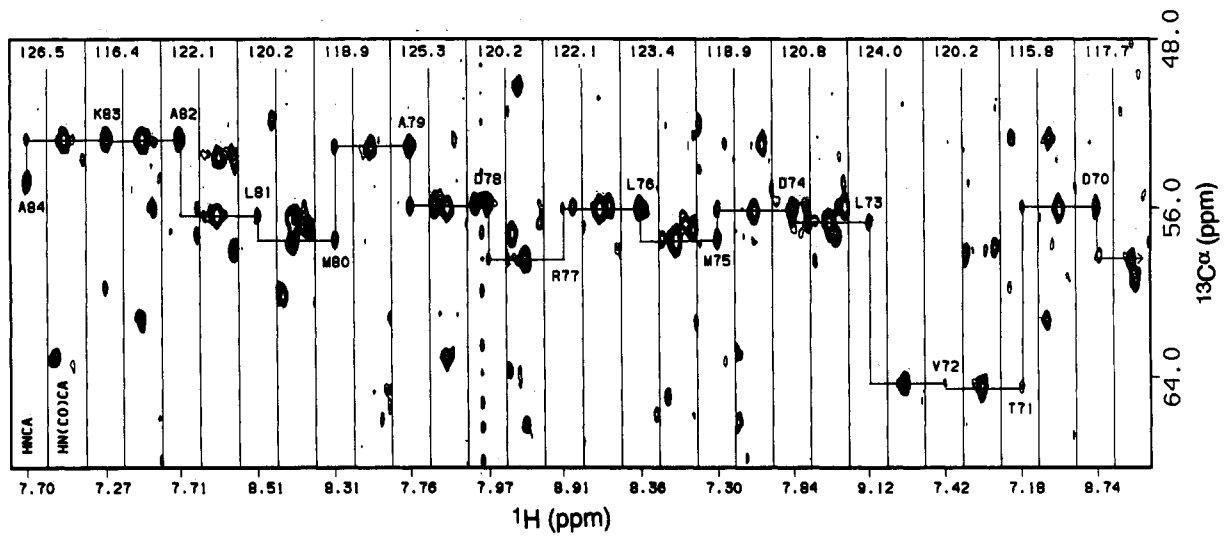

FIGURE 4: Selected ^{15}N chemical shift slices from the 3D HNCA and HN(CO)CA spectra. The sequential pathway for the Ala84–Asp70 peptide stretch is illustrated. The ^{15}N chemical shifts are indicated at the top of each panel. Intraresidue $^1H^N$–^{15}N–$^{13}C^\alpha$ correlation peaks are labeled with the corresponding residue numbers in the HNCA spectra. The sequential connectivity to Leu69 cannot be obtained from these 3D data because the HNCA cross peak of the residue was undetectable.

Leu, Ile, and aromatic residues were identified from the analysis of homonuclear 2D COSY, NOESY, and TOCSY spectra. In addition, ca. 70 out of 200 expected H^N–H^α cross peaks were observed in COSY and TOCSY spectra.

(B) 2D HMQC and HMQC-NOESY Experiments. Figure 1 shows the 2D ^1H–^{15}N HSMQC spectrum of uniformly labeled [^{15}N]AK complexed to $MgAP_5A$. Although some spectral overlap due to relatively poor dispersion of H^N and ^{15}N resonances is apparent, almost all of the expected ^{15}N–H cross peaks are observed. Many of these cross peaks could easily be assigned by obtaining ^1H–^{15}N HMQC (or HSMQC) spectra of selectively labeled AK samples, as will be described in a later section. The assignments, taken together with the spin system information from the homonuclear 2D data, provided information necessary for subsequent sequential assignments derived from heteronuclear 2D and 3D NMR data. In addition, we also searched for the consecutive $d_{NN(i,i+1)}$ NOEs using 2D HMQC-NOESY, which allowed us to verify and extend the sequential assignments determined from other data. The ^{15}N chemical shift information thus obtained was useful later in identifying corresponding NOEs in 3D NOESY-HMQC spectra.

(C) 3D Experiments. The 3D NOESY-HMQC spectrum was searched for $d_{\alpha N(i,i+1)}$ NOEs, but these NOEs could only be identified unambiguously when they arose from well-resolved H^α resonances. We then used the triple-resonance HNCA and HN(CO)CA 3D data to verify all sequential connectivities obtained from $d_{NN(i,i+1)}$ and $d_{\alpha N(i,i+1)}$ NOEs. The other triple-resonance 3D experiments such as HNCO, HN(CA)HA, and ^{15}N TOCSY-HMQC were not used directly for sequential assignments, but were used to obtain chemical shifts for the carbonyl carbon ($^{13}C'$), H^α, and H^β resonances; this information helped indirectly with the assignments.

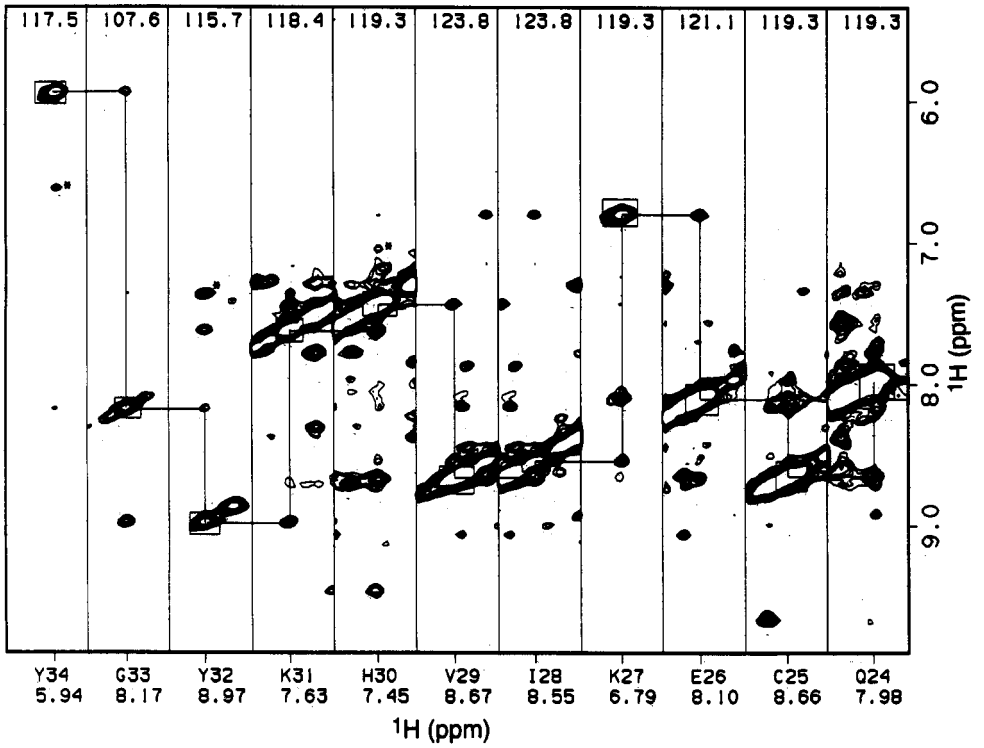

FIGURE 5: Sequential assignments for Tyr34–Gln24 from $d_{NN(i,i+1)}$ NOE connectivities found in the 3D ^{15}N NOESY-HMQC data (t_{mix} = 0.12 s). Slices were taken at specific ^{15}N chemical shifts shown at the top of each panel. Residue number and amide proton chemical shifts are indicated below each panel. The H^N diagonal peaks are boxed, and the sequential $d_{NN(i,i+1)}$ NOE connectivities are indicated by lines. Intraresidue NOEs to the corresponding aromatic ring H^δ protons are indicated with *.

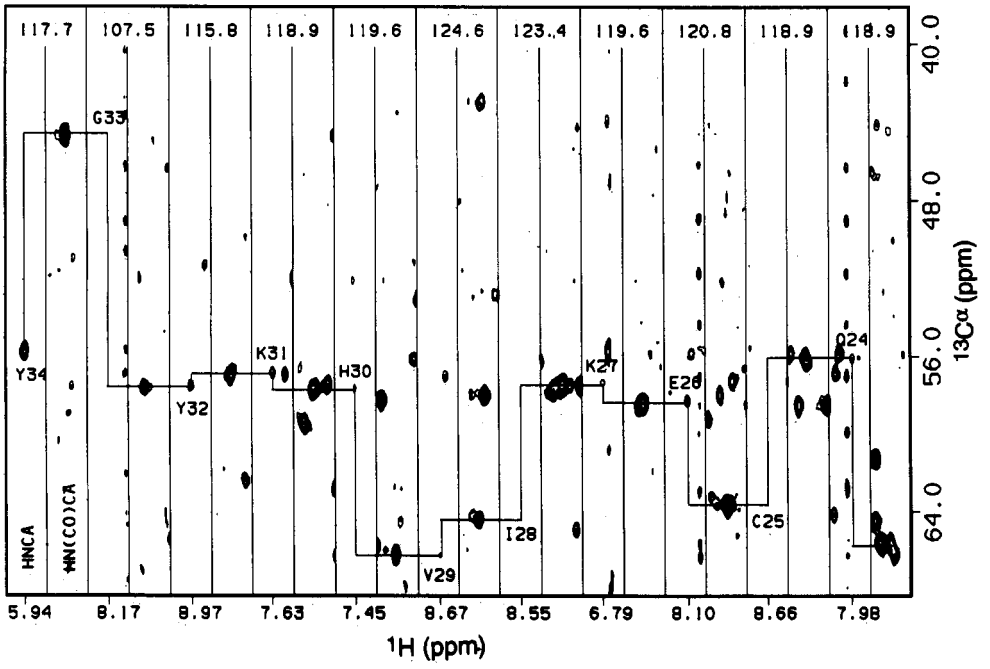

FIGURE 6: Selected ^{15}N chemical shift slices from the 3D HNCA and HN(CO)CA spectra. The sequential assignment pathway for the Tyr34–Gln24 peptide stretch is illustrated. The ^{15}N chemical shifts are indicated at the top of each panel. Intraresidue $^1H^N$–^{15}N–$^{13}C^\alpha$ correlation peaks are labeled with the corresponding residue numbers in the HNCA spectra.

Specific Assignments from Specifically Labeled AK. Five AK samples labeled with specific [^{15}N]- and/or [$^{13}C'$]amino acids were used to identify specific N–H cross peaks in Figure 1: (i) As shown in Figure 2A, the ^1H–^{15}N HMQC spectrum of the [^{15}N]Leu/[$^{13}C'$]Val-labeled AK sample exhibited resolved ^{15}N–H cross peaks from all 20 leucine residues; that of Leu73 was easily identified by splitting due to coupling with the carbonyl carbon of the preceding Val residue, Val72. (ii) Similarly, ^1H–^{15}N HMQC cross peaks were observed from all 15 valine residues in the spectrum of the [^{15}N]Val/[$^{13}C'$]-Leu-labeled AK; here, the Val67 cross peak was readily identified from resolved coupling to the preceding residue, Leu66 (Figure 2B). A few very weak cross peaks were also observed, which indicated some transfer of the label to other amino acids. These weak peaks were found to arise from either alanine or isoleucine on the basis of other experiments. (iii) Twenty-one out of twenty-two Lys cross peaks were detected in the HSMQC spectrum of the [^{15}N]Lys/[$^{13}C'$]-Leu-labeled AK sample (Figure 2C). Signals from Lys6 and Lys131 were identified on the basis of coupling to the labeled

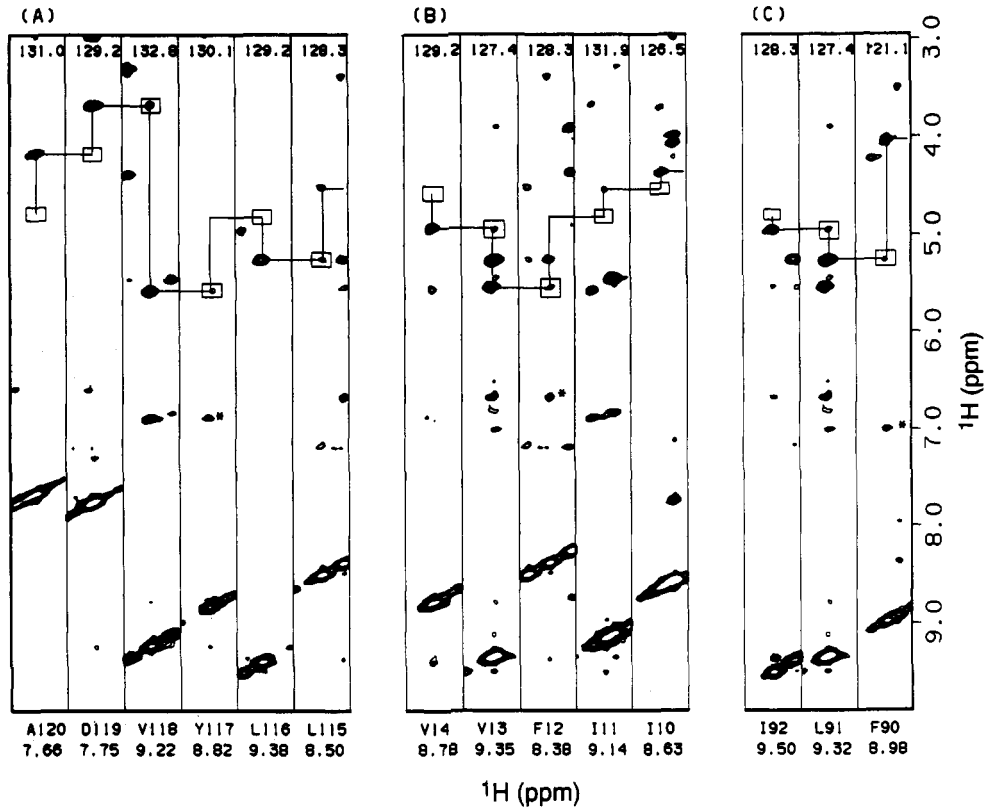

FIGURE 7: Sequential assignments for (A) Ala120–Leu115, (B) Val14–Ile10, and (C) Ile92–Phe90 from $d_{\alpha N(i,i+1)}$ NOE connectivities found in the 3D ^{15}N NOESY-HMQC data (t_{mix} = 0.12 s). Slices were taken at the specific ^{15}N chemical shifts shown at the top of each panel. Assigned residue numbers and amide proton chemical shifts are indicated below each panel. The intraresidue $d_{\alpha N}$ NOE peaks are indicated with boxes, and the sequential $d_{\alpha N(i,i+1)}$ NOE connectivities are indicated by lines. Intraresidue NOEs between H^N and the corresponding aromatic ring H^δ protons are indicated with *. Note that the water signal resonates at ca. 4.7 ppm; cross peaks near this chemical shift were bleached out in these spectra. Some of the missing cross peaks, however, were clearly observed in the NOESY spectrum in D_2O.

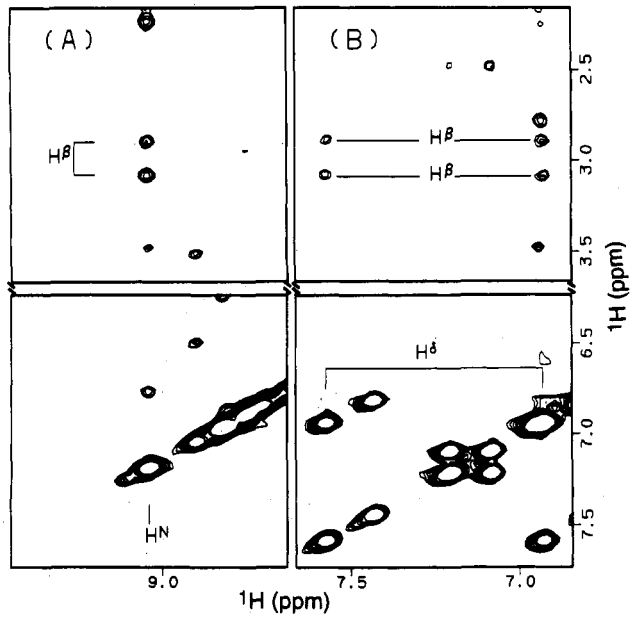

FIGURE 8: Assignment of the side-chain $^1H^\delta$ protons of Asn174 from the 3D ^{15}N NOESY-HMQC data. Slices were taken at the specific ^{15}N chemical shifts: 122.9 ppm for A and 113.0 ppm for B. The $^1H^N$ (A) and both $^1H^\delta$ (B) protons were observed to have NOEs to the $^1H^\beta$ protons.

carbonyl carbon of the preceding Leu residues (Leu5 and Leu130, respectively). Note that the Lys4 and Lys107 cross peaks are overlapped. This overlap, however, was clearly resolved in the 3D HNCO and HNCA spectra. (iv) The [^{15}N]Gly/[^{15}N]Ser/[$^{13}C'$]Val-labeled AK prepared by using *E. coli* strain DL49SPH as the host bacterium yielded serious transfer of the label to the side-chain NH_2 groups of Asn and/or Gln (data not shown). However, the sample was still useful for identifying the majority of Gly (11 out of 19) and Ser (5 out of 9) residues. Gly15 and Ser48 were easily assigned on the basis of coupling to the labeled carbonyl carbon of the preceding valine residues (Val14 and Val47, respectively). (v) Later, we succeeded in selectively labeling AK with [^{15}N]-Gly using the DL39G strain, auxotrophic to glycine, and therefore were able to identify the 11 glycines (Figure 2D).

Sequential Assignments from 2D and 3D Heteronuclear Data. Table II lists the assigned chemical shifts of ca. 90% of the backbone nuclei ^{15}N, H^N, $^{13}C'$, $^{13}C^\alpha$, and H^α resonances and ca. 40% of the side-chain protons. Details of the assignment procedures are illustrated by the following representative examples.

(A) The Ala84–Leu69 Stretch with Strong $d_{NN(i,i+1)}$ NOEs. Figure 3 shows the $d_{NN(i,i+1)}$ NOE connectivities for the Ala84–Leu69 stretch observed in the 3D NOESY-HMQC spectrum, while Figure 4 shows the sequential connectivities for the same stretch found in the HNCA and HN(CO)CA spectra. The sequential assignments were based on the following criteria: (i) The HMQC experiment with [^{15}N]Leu/[$^{13}C'$]Val-labeled AK (Figure 2A) identified the fourth, ninth, twelfth (Figures 3 and 4), and last panels (Figure 3) as leucines and the twelfth panel as Leu73. (ii) The thirteenth panel in Figures 3 and 4 was assigned to valine from the HMQC experiments of [^{15}N]Val/[$^{13}C'$]Leu-labeled AK (Figure 2B). The COSY and TOCSY spectra also confirmed its identification as valine. (iii) The first, third, and sixth panels in Figures 3 and 4 were identified as Ala from the COSY and TOCSY data. Note that the first (Ala84) and sixth (Ala79) residues were also observed as weak cross peaks from the HMQC spectrum of the [^{15}N]Val/[$^{13}C'$]Leu-labeled AK (Figure 2B) as the result of metabolic migration of the label. (iv) Only the Ala84–

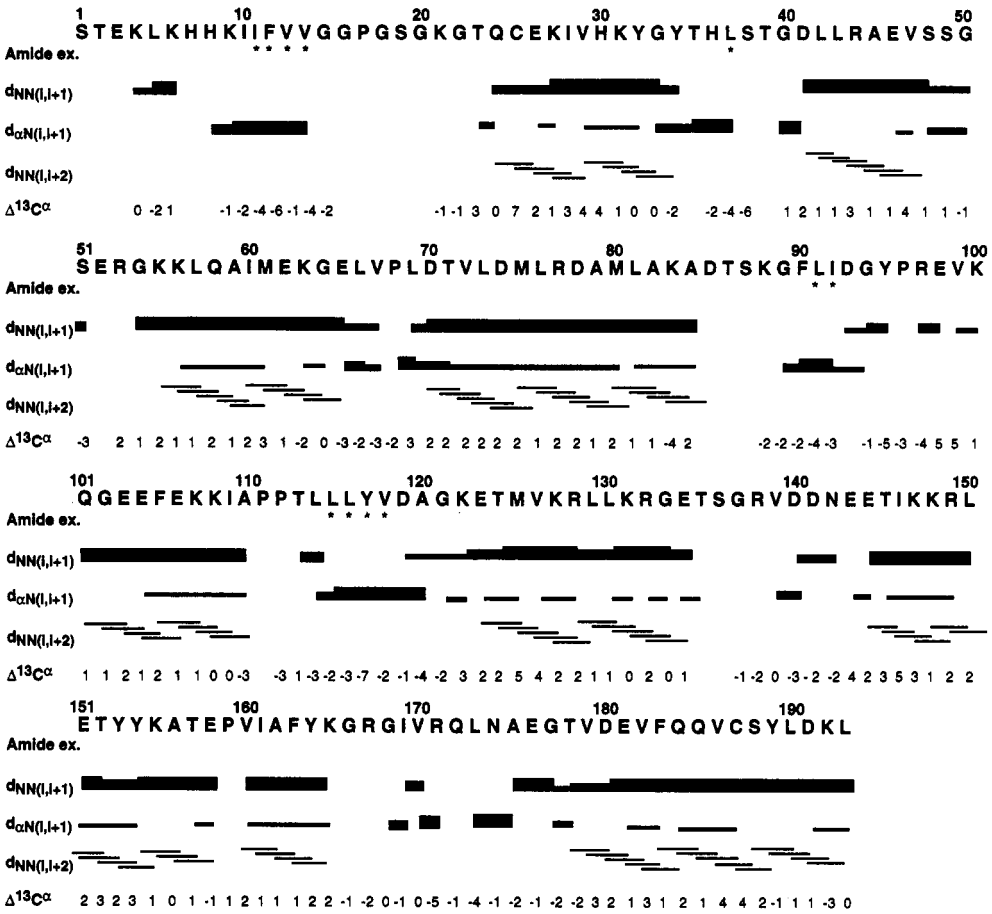

FIGURE 9: Summary of sequential and $d_{NN(i,i+2)}$ NOEs and the $\Delta^{13}C^{\alpha}$ values. The thickness of the lines corresponds to the cross peak intensity. Deviations from the random-coil values of the $^{13}C^{\alpha}$ chemical shifts are shown as $\Delta^{13}C^{\alpha}$. The amide protons that were still present after incubation for 1 week in D_2O are marked by *.

Leu69 polypeptide sequence in AK satisfies these primary sequence criteria, leading us to assign the $d_{NN(i,i+1)}$ NOE connectivities to this sequence. (v) Analyses of the triple-resonance HNCA and HN(CO)CA 3D data confirmed the assignments for Ala84–Leu69 (Figure 4). Note that the sequential connectivities obtained from these two triple-resonance experiments alone cannot provide unambiguous assignments. However, when combined with the NOE connectivity data, they became much more effective in yielding sequential assignments. For example, whenever there is any ambiguity in sequential NOE connectivities (even in 3D NOESY-HMQC) resulting from resonance overlap, it can be easily resolved on the basis of connectivities from the triple-resonance data. (vi) The $^{13}C^{\alpha}$ chemical shifts can also be used as a qualitative measure to verify the assignments since particular residue types exhibit characteristic $^{13}C^{\alpha}$ values (Spera & Bax, 1991). For example, the $^{13}C^{\alpha}$ resonances of Thr, Val, and Ile are relatively downfield (ca. 62 ppm), whereas those for Ala (ca. 52 ppm) and Gly (ca. 45 ppm) are relatively upfield. Note that the $^{13}C^{\alpha}$ chemical shifts assigned to the residues in the Ala84–Leu69 sequence (Table II) satisfy these criteria.

(B) The Tyr34–Gln24 Stretch with Strong $d_{NN(i,i+1)}$ NOE. Figure 5 shows another example of consecutive $d_{NN(i,i+1)}$ NOE connectivities (Tyr34–Gln24). Assignments for this sequence were achieved by using essentially the same strategy as for the Ala84–Leu69 sequence: The HMQC and HSMQC data on the specifically labeled AK samples shown in Figure 2 unambiguously identified the second panel as Gly, the fourth and eighth panels as Lys, and the sixth panel as Val. Sequential connectivities obtained from NOE data were verified by HNCA and HN(CO)CA connectivities shown in Figure 6. The $^{13}C^{\alpha}$ values for the sequence fall into the chemical shift regions characteristic of individual residue types (Spera & Bax, 1991). In addition, the H^N protons of the aromatic residues in this sequence (Tyr34, Tyr32, and His30) exhibited intraresidue NOEs to the corresponding H^{δ} protons, which provided additional evidence for the proposed assignments.

Approximately 70% of the AK sequence showed relatively strong sequential $d_{NN(i,i+1)}$ NOEs. Thus, sequential assignments for 70% of the AK sequence were obtained by using procedures similar to those used in examples A and B.

(C) Three Short Stretches with Strong $d_{\alpha N(i,i+1)}$ NOE. Figure 7 shows the $d_{\alpha N(i,i+1)}$ NOE connectivities for three short stretches: Ala120–Leu115, Val14–Ile10, and Ile92–Phe90. These stretches exhibited NOE patterns characteristic of β-sheet structures (see the Identification of Secondary Structures section). The $d_{\alpha N(i,i+1)}$ NOEs involved in the sequence can be unambiguously assigned because most of their α-protons resonated in a well-resolved region, downfield from the water resonance. Sequential assignments for these stretches were achieved by essentially the same strategy as described in A and B, except for the use of $d_{\alpha N(i,i+1)}$ NOEs instead of $d_{NN(i,i+1)}$ NOEs. The HMQC experiments on the specifically labeled AK samples (Figure 2) allowed assignment of the third panel of Figure 7A and the first and second panels of Figure 7B to valines and of the fifth and sixth panels of Figure 7A and the second panel of Figure 7C to leucines. The H^N protons of the aromatic residues in the stretches (Tyr117, Phe12, and Phe90) showed intraresidue NOEs with the corresponding aromatic H^{δ} protons. In addition, the sequential assignments obtained from $d_{\alpha N(i,i+1)}$ NOEs were verified by HNCA and HN(CO)CA data (not shown). The strategy described here was used to assign ca. 20% of the AK sequence.

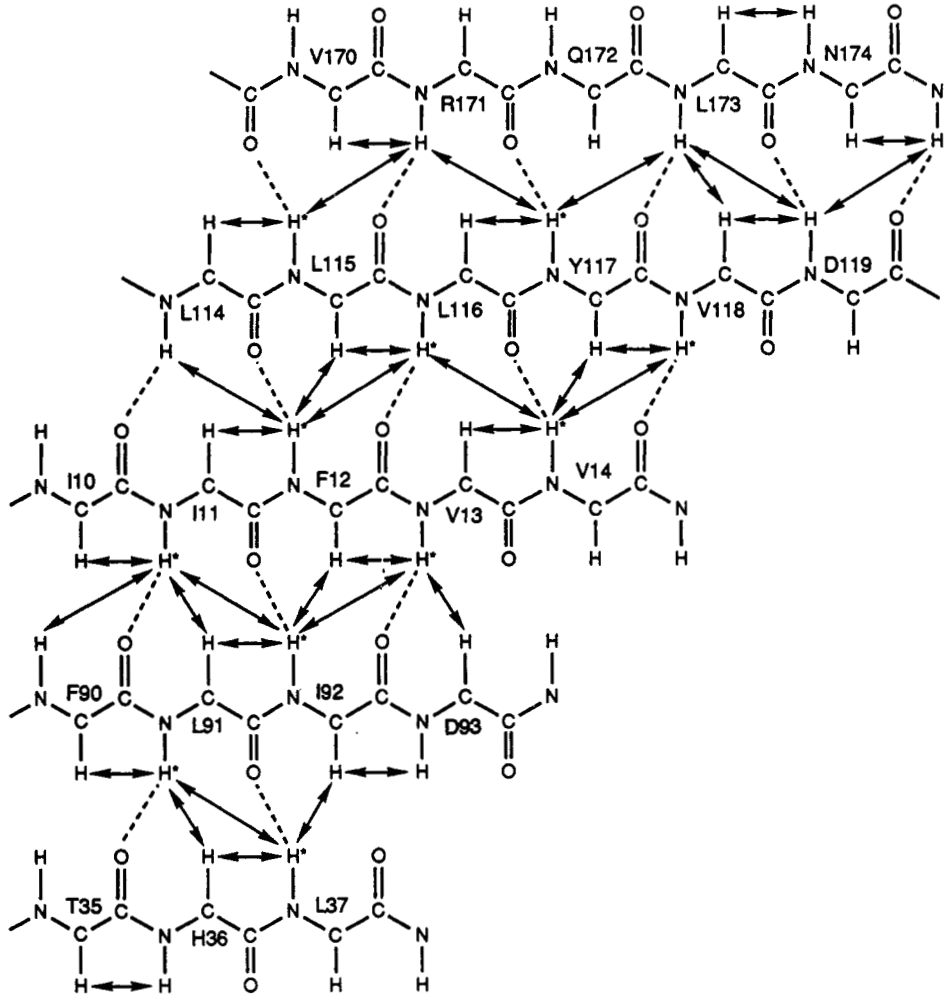

FIGURE 10: Predicted parallel β-sheet structure in AK·$MgAP_5A$. The identified NOEs are denoted by arrows (↔). Possible hydrogen bonds are indicated by dashed lines (- - -). The amide protons that were still present after incubation for 1 week in D_2O are marked by *.

(D) Assignment of Side-Chain Protons. Although complete side-chain assignments have not been achieved at this stage of the analysis, ca. 40% of side-chain protons have been assigned, as listed in Table II. The assignments were based mainly on spin system identifications by 2D COSY, NOESY, and TOCSY and 3D ^{15}N TOCSY-HMQC, HN(CA)HA, ^{13}C HCCH-TOCSY, and HCCH-COSY data. The side-chain $^1H^\delta$ and $^1H^\epsilon$ proton resonances of Asn and Gln residues, respectively, were readily differentiated from the backbone $^1H^N$ protons, since in the 3D NOESY-HMQC experiment they appear as paired peaks at the same ^{15}N frequency and display intense NOEs between the paired peaks. The backbone $^1H^N$ resonances of Asn and Gln were matched to corresponding side-chain $^1H^\delta$(Asn) or $^1H^\epsilon$(Gln) resonances on the basis of mutual NOEs to H^β(Asn) or H^γ(Gln) resonances. Figure 8 illustrates such NOEs for Asn174. This strategy led to assignments of the side-chain resonances of the two asparagines and three of the six glutamines (Table II).

Identification of Secondary Structures. Helical structures are characterized by strong consecutive $d_{NN(i,i+1)}$ NOEs and weak–medium-range NOEs such as $d_{NN(i,i+2)}$, $d_{\alpha N(i,i+2)}$, $d_{\alpha N(i,i+3)}$, $d_{\alpha\beta(i,i+3)}$, and $d_{\alpha N(i,i+4)}$ (Wagner et al., 1986; Wüthrich, 1986). Because the H^α protons in helical structures, in general, resonate in a highly crowded and degenerate region (4.0–4.5 ppm), it was not possible to unambiguously assign all of the $d_{\alpha N}$ NOEs from the 3D ^{15}N NOESY-HMQC data alone. However, the $d_{NN(i,i+2)}$ NOEs could be identified unambiguously from the available 3D NOESY-HMQC data. These NOE data suffice for the detection of helices, but do not permit their further classification by helix type.

The β-sheet structures are known to display three NOE patterns: strong consecutive $d_{\alpha N(i,i+1)}$ NOEs, weak intraresidue $d_{\alpha N}$ NOEs, and long-range NOEs between strands showing strong consecutive $d_{\alpha N(i,i+1)}$ NOEs. The patterns of long-range interstrand NOEs can also determine the types of β-sheet structures: strong interstrand H^α–H^α NOEs as well as weak interstrand H^α–H^N and H^N–H^N NOEs are expected for antiparallel β-sheets, while only the weak interstrand H^α–H^N and H^N–H^N NOEs are expected for parallel β-sheets (Wüthrich, 1986).

A recent publication by Spera and Bax (1991) has shown that the deviation from random-coil $^{13}C^\alpha$ chemical shifts ($\Delta^{13}C^\alpha$) can be qualitatively correlated with secondary structure: the $^{13}C^\alpha$ resonances of residues in α-helical structures are downfield-shifted compared to those in random-coil structures (i.e., $\Delta^{13}C^\alpha > 0$), while those in β-sheets are upfield-shifted ($\Delta^{13}C^\alpha < 0$). Since $^{13}C^\alpha$ chemical shifts are available for most of the AK residues (Table II), the $\Delta^{13}C^\alpha$ values were used to verify the secondary structures determined from NOE data. Figure 9 summarizes all of the observed sequential and $d_{NN(i,i+2)}$ NOE connectivities, amide exchange rates, and $\Delta^{13}C^\alpha$ data.

On the basis of the criteria described above, the AK data were searched for information about secondary structural elements. As shown in Figure 3, the Ala84–Leu69 stretch exhibits strong consecutive $d_{NN(i,i+1)}$ NOEs, which indicate that the stretch can be assigned to a helical structure. A search for weak $d_{NN(i,i+2)}$ NOEs confirmed the helical structure: $d_{NN(i,i+2)}$ NOEs were clearly observed between Ala82 and Met80, Leu81 and Ala79, and Asp74 and Val72

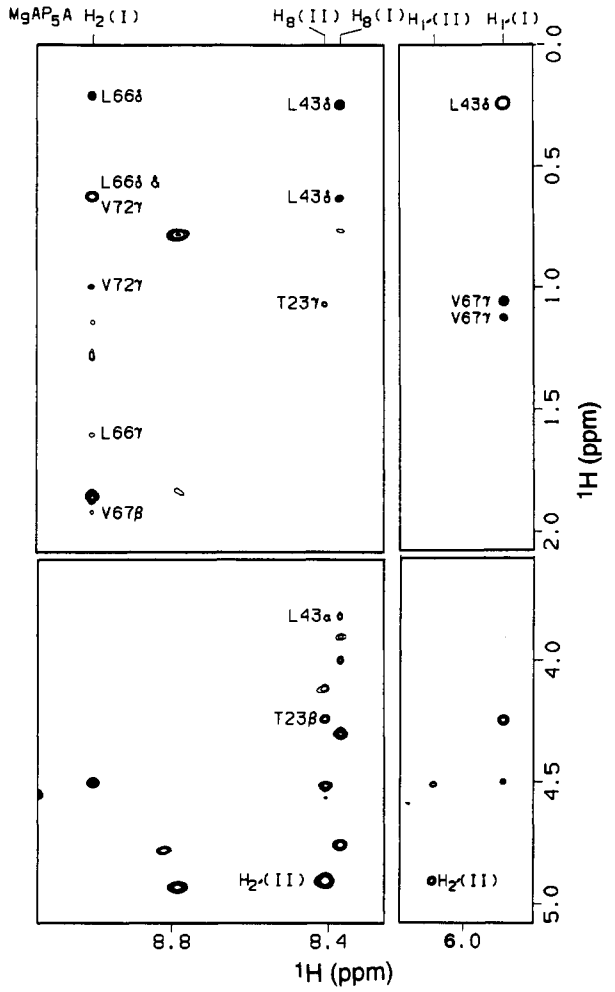

FIGURE 11: Partial 2D NOESY spectrum (t_{mix} = 0.12 s) of AK·MgAP5A in D_2O at 500 MHz, showing NOE cross peaks between adenosine resonances (H_2, H_8, and $H_{1'}$) and aliphatic side chains. I and II designate the AMP and ATP moieties, respectively, of MgAP5A. No NOE was observed for H_2(II), which resonates at 8.32 ppm.

(Figure 3). Note, however, that several expected $d_{NN(i,i+2)}$ NOEs were too weak to be detected at the contour levels shown in Figure 3; these were clearly observed at lower contour levels. Similarly, the Tyr34–Gln24 sequence also exhibited strong consecutive $d_{NN(i,i+1)}$ NOEs (Figure 5) and weak $d_{NN(i,i+2)}$ NOEs (Figure 9), which permitted the assignment of this sequence to a helical structure. Helical structures were also identified for the following stretches of AK: Asp41–Ser48, Lys55–Glu65, Gln101–Ala110, Glu123–Glu134, Glu144–Glu158, Val160–Lys165, and Thr178–Leu193.

The polypeptide stretches showing consecutive strong sequential $d_{\alpha N(i,i+1)}$ NOE connectivities are shown in Figures 7 and 9. These stretches were searched for possible long-range ($|i - j| \geq 5$) NOEs. A five-stranded parallel β-sheet consisting of segments Thr35–Leu37, Phe90–Asp93, Ile10–Val14, Leu114–Asp119, and Val170–Ala175 was identified (Figure 10). Note that the last stretch was assigned as a β-strand on the basis of many interstrand NOEs shown in Figure 10, despite a break in the sequential $d_{\alpha N(i,i+1)}$ NOE connectivities for the Arg171–Leu173 segment. The break was caused primarily by the fact that the H^α resonances of Arg171 and Gln172 were undetectable, possibly because they overlapped with the water signal. Note that most of the backbone H^N protons involved in the β-sheet structures showed retarded H–D exchange kinetics (Figures 9 and 10), indicating that they experience little solvent exposure. The results agree well with the X-ray structure of substrate-free porcine AK, which shows a central five-strand parallel β-sheet surrounded by several α-helices (Schulz et al., 1974; Dreusicke et al., 1988).

Note that strikingly good correlations were observed between the secondary structures and the $\Delta^{13}C^\alpha$ values (Figure 9): most of the AK residues in helical structures show positive (downfield-shifted) $\Delta^{13}C^\alpha$ values, whereas residues in β-sheets show negative (upfield-shifted) $\Delta^{13}C^\alpha$ values.

Intermolecular AK·MgAP5A Contact Points. Although the sequence-specific assignments are not complete and the tertiary structure is yet to be determined, it has been possible to identify intermolecular NOEs between AK and MgAP5A resonances. Although free AP5A is a symmetrical molecule, it displays two distinct sets of adenosine signals when bound to AK. This indicates that the lifetime of the complex is long on the chemical shift time scale and that the bound environments at the AMP site and the MgATP site are different. The detailed assignments of the MgAP5A protons have been reported in our previous publications (Yan et al., 1990; Shi et al., 1993). The 2D NOESY in D_2O exhibited a number of NOEs between these MgAP5A resonances and AK signals, as shown in Figure 11. Most of these NOE cross peaks were assigned on the basis of the known chemical shifts of AK residues. NOEs involving H^N protons were identified from the 3D NOESY-HMQC spectrum in ^1H_2O. The results are summarized in Figure 12. It is apparent that the adenosine of the ATP moiety of MgAP5A shows substantially fewer NOE cross peaks than the AMP moiety; the only residue identified to exhibit an NOE with ATP is Thr23. In contrast, the AMP moiety exhibits many more contact points with AK: Thr39, Leu43, Gly64, Leu66, Val67, Val72, and Gln101 all display NOEs with the AMP moiety of MgAP5A.

DISCUSSION

Total Assignment of AK·MgAP5A. Since our long-term objective is to correlate the structure of AK with its mechanism of catalysis, we were fortunate to be able to conduct assignments at pH 7.1, where the catalytic activity is optimal. The amide protons of all but 19 non-proline residues were observed in the ^1H–^{15}N HSMQC spectrum even at neutral pH (Figure 1). As shown in Figure 1, severe crowding occurs in the region 116–124 ppm for ^{15}N and 7.2–8.7 ppm for H^N resonances. However, these overlaps were resolved in the 3D HNCO, HNCA, and HN(CO)CA spectra. Overall, we have assigned over 90% of the backbone (^{15}N, H^N, $^{13}C^\alpha$, H^α, $^{13}C'$) and ca. 40% of the side-chain resonances (Table II).

Of the 19 non-proline residues that did not show detectable ^1H–^{15}N cross peaks in the HSMQC experiment, three lie in the N-terminal region (Ser1–Glu3), which is likely to have greater flexibility. The remaining unassigned residues are located in loop regions in the crystal structure of free AK1 (Pai et al., 1977; Dreusicke et al., 1988). Most noticeable is the segment, ^{16}GPGSG^{20}, in the P loop region, which is intimately involved in catalysis and is of great interest to us. It is uncertain whether these H^N protons can be observed under different conditions such as acidic pH, low temperature, or the substrate-free enzyme.

Secondary Structure in the AK·MgAP5A Complex. Figure 13 compares the secondary structures of free porcine muscle AK in the crystal form (Dreusicke et al., 1988) and that of chicken muscle AK·MgAP5A in solution (this work). Essentially the same helices and β-sheets exist in the two systems, but small differences occur in the actual starting and ending residues for each secondary structural element. For example, the second helix consists of residues 20–33 in the free enzyme crystal and residues 24–34 in the complex in solution, and the

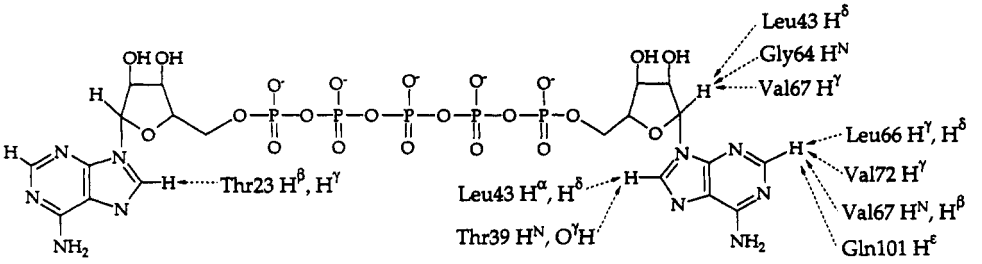

FIGURE 12: Summary of intermolecular NOEs between AK residues and the adenosine moieties of AP_5A.

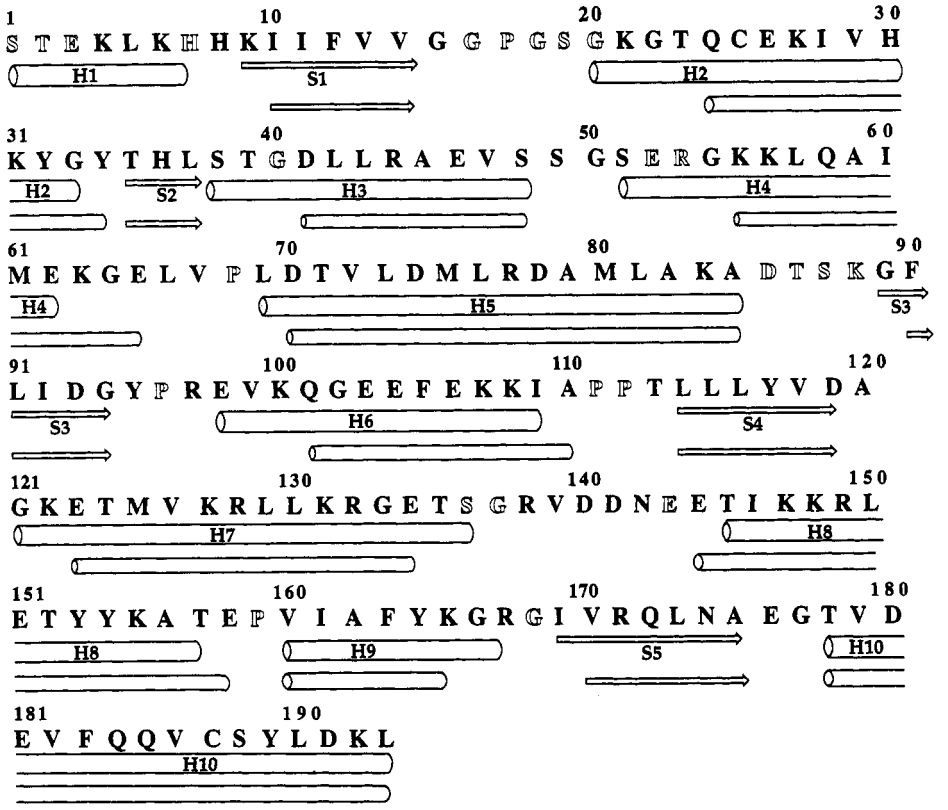

FIGURE 13: Comparison between the secondary structures of free porcine muscle AK in the crystal form and chicken muscle AK·$MgAP_5A$ in solution. The first line gives the amino acid sequence of chicken muscle AK; residues assigned in this article are labeled with solid letters, and residues that remain unassigned are represented by outlined letters. The second line represents the secondary structure found in the 2.1-Å X-ray model of porcine muscle AK (Dreusicke et al., 1988). The third line shows the secondary structure of chicken mucsle AK·$MgAP_5A$ in solution determined from the NMR results presented in this article. H and S represent helix and β-sheet, respectively.

fourth helix involves residues 51–62 in the former and 55–65 in the latter. Another difference occurs in the N-terminal region: in the free enzyme crystal, the first seven N-terminal residues are part of a helix, whereas in AK1·$MgAP_5A$ in solution they show a disordered structure. These differences in the secondary structure may result from differences in the physical form (solid vs solution), the complexation state (free vs $MgAP_5A$-bound), or the species (porcine vs chicken).

Regions not identified as helices or β-sheets are likely to be loops. These loop structures in solution probably will not be defined until the tertiary structure can be solved. Since the free enzyme and the complexed form consist of very similar secondary structural elements, as shown in Figure 13, and since AK is known to undergo large conformational changes during catalysis (Schulz, 1992), the loops are likely to play important roles in conformational changes during catalysis.

Substrate Sites of Muscle AK. Many residues have been implicated as interacting with the phosphate groups of AMP and ATP on the basis of our site-directed mutagenesis studies of AK1, but relatively little is known regarding the adenosine moiety of either substrate (Yan & Tsai, 1991). Although we have not yet solved the tertiary structure of the AK1·$MgAP_5A$ complex in solution, most of the NOE cross peaks between the adenosine resonances and the AK residues have been assigned (Figure 11), and the results summarized in Figure 12 are sufficient to warrant comparisons with various previous studies on the subject.

(A) Comparison with the Results of Site-Directed Mutagenesis. Not all of the residues in Figure 12 have been examined by site-directed mutagenesis, and not all of the residues examined may reveal a functional role, since a residue in proximity to a substrate is not necessarily functional. Nonetheless, mutants of Leu66 (Okajima et al., 1991) and Gln101 (unpublished results) have been shown to display significant increases in the K_m of AMP (but not MgATP) and significant decreases in k_{cat}. On the other hand, no mutant displaying a specific effect on the K_m of MgATP has yet been identified. The side chain of Thr23 displays strong NOEs with the ATP adenosine moiety, but its functional role is to interact with the α-phosphoryl group (Shi et al., 1993).

(B) Comparison with Previous NMR Analyses. On the basis of partial assignments of aromatic residues, Rösch and

co-workers examined possible interactions between the adenosine moieties of $MgAP_5A$ and the aromatic side chains of AKe (Vetter et al., 1990) or AKy (Vetter et al., 1991). No aromatic side chains were found to be in contact with the AMP moiety in either case. In both cases a residue in the 30-residue insertion segment, which is absent in AK1, was identified to be in proximity to the ATP adenosine moiety. In addition, one other residue was shown to be in proximity to ATP adenosine: Phe19 in AKe (corresponding to Lys27 in AK1) and Trp210 in AKy (corresponding to Phe183 in AK1). Neither was found in our results with AK1; however, the residue identified in our results, Thr23, is close to Lys27.

(C) Comparison with the Crystal Structure. The most current crystal structure is that of the AKe·AP_5A complex at 1.9-Å resolution (Müller & Schulz, 1992). The residues proximal to the AMP adenine ring deduced from the present article agree almost entirely with those in the crystal structure. The only notable difference is that Tyr95 was identified in the crystal structure but not in the NMR study. This difference can be fully explained. In the crystal structure, the closest distance, 3.62 Å, is between the H^{δ} of residue 95 and the NH_2 group of the adenine ring. The NH_2 protons were not assigned in NMR, and all other protons of the adenine ring lie beyond the 4-Å range. Thus, our results strongly indicate that the AMP–AK binding interactions are essentially the same for AKe·AP_5A in crystals and AK1·$MgAP_5A$ in solution. On the other hand, some uncertainty remains for the MgATP site: some of the interactions in the crystal structure involve the 30-residue insertion segment not present in AK1, and other interactions (involving residues 175, 177–179, and 182) were not found in the NMR results. Thr23, which was suggested to hydrogen bond the α-phosphate of ATP from the results of both mutagenesis (Shi et al., 1993) and X-ray (Müller & Schulz, 1992) analyses, was found to be in proximity to the ATP adenosine moiety in the NMR study (Shi et al., 1993), but not in the crystal structure (Müller & Schulz, 1992).

Although we have assigned most of the NOE cross peaks, we have not yet exhausted all possibilities, and efforts are still in progress to identify more NOEs between the ATP adenosine and AK.

Implications for the Mechanism of Catalysis. The adenosine of the AMP moiety shows a large number of interactions with the enzyme. In contrast, the adenosine in the ATP moiety shows very few points of contact with the enzyme: only the Thr23 CH^{β} and $CH^{\gamma}{}_3$ protons interact with the adenine H_2 and the ribose $H_{1'}$ protons. The results provide an explanation of why AK shows much more stringent substrate specificity at the AMP site than at the MgATP site (Noda, 1973; Tomasselli & Noda, 1980).

If the AMP site displays more extensive and stringent enzyme–substrate interactions, how can we rationalize the fact that the K_d and K_m values of AMP are ca. 2-fold higher than the corresponding values of MgATP (Tian et al., 1988)? As demonstrated previously, the binding energy of MgATP mainly comes from binding of the triphosphate moiety (Sanders et al., 1989).

REFERENCES

Bax, A., & Davis (1985) *J. Magn. Reson. 65*, 355–360.

Bax, A., & Ikura, M. (1991) *J. Biomol. NMR 1*, 99–104.

Bax, A., Clore, G. M., Driscoll, P., Gronenborn, A. M., Ikura, M., & Kay, L. E. (1990a) *J. Magn. Reson. 87*, 620–627.

Bax, A., Clore, G. M., & Gronenborn, A. M. (1990b) *J. Magn. Reson. 88*, 425–431.

Bax, A., Ikura, M., Kay, L. E., & Zhu, G (1991) *J. Magn. Reson. 91*, 174–178

Bodenhausen, G., Kogler, H., & Ernst, R. R. (1984) *J. Magn. Reson. 58*, 370–388.

Clubb, R. J., Thanabal, V., Osborne, C., & Wagner, G. (1991) *Biochemistry 30*, 7718–7730.

Clubb, R. J., Thanabal, & Wagner, G. (1992) *J. Biomol. NMR 2*, 203–210.

Dahnke, T., & Tsai, M.-D. (1993) *J. Biol. Chem.* (submitted for publication).

Diederichs, K., & Schulz, G. E. (1991) *J. Mol. Biol. 217*, 541–549.

Dreusicke, D., Karplus, P. A., & Schulz, G. E. (1988) *J. Mol. Biol. 199*, 359–371.

Drobny, G., Pines, A., Sinton, S., Weitekamp, D., & Wemmer, D. (1979) *Faraday Div. Chem. Soc. Symp. 13*, 49.

Egner, U., Tomasselli, A. G., & Schulz, G. E. (1987) *J. Mol. Biol. 195*, 649–658.

Gerstein, M., Schulz, G. E., & Chothia, C. (1993) *J. Mol. Biol. 229*, 494–501.

Ikura M., Kay L. E., & Bax, A. (1990) *Biochemistry 29*, 4659–4667.

Marion, D., & Wüthrich, K. (1983) *Biochem. Biophys. Res. Commun. 113*, 967–974.

Marion, D., & Bax, A. (1989) *J. Magn. Reson. 83*, 205–211.

Marion, D., Driscoll, P. C., Kay, L. E., Wingfield, P. T., Bax, A., Gronenborn, A., & Clore, G. M. (1989a) *Biochemistry 28*, 6150–6156.

Marion, D., Ikura, M., Tschudin, R., & Bax, A. (1989b) *J. Magn. Reson. 85*, 393–399.

McCoy, M. A., & Muller, L. (1992) *J. Magn. Reson. 99*, 18–36.

Mooberry, E. S., Edison, A. S., Abildgaard, F., Markley, J. L., Byeon, I.-J. L., & Tsai, M.-D. (1992) in *Proceedings of the International Symposium on Spectroscopy and Structure of Molecules and Nuclei* (Johnson, N. R., Shelton, W. N., & El-Sayed, M., Eds.) pp 375–380, World Scientific, Singapore.

Muchmore, D. C., McIntosh, L. P., Russell, C. B., Anderson, D. E., & Dahlquist, F. W. (1989) *Methods Enzymol. 177*, 44–73.

Mueller, L. (1979) *J. Am. Chem. Soc. 101*, 4481–4484.

Müller, C. W., & Schulz, G. E. (1992) *J. Mol. Biol. 224*, 159–177.

Noda, L. (1973) *The Enzymes (3rd Ed.) 7*, 279–305.

Okajima, T., Tanizawa, K., Yoneya, T., & Fukui, T. (1991) *J. Biol. Chem. 266*, 11442–11447.

Pai, E. F., Sachsenheimer, W., Schirmer, R. H., & Schulz, G. E. (1977) *J. Mol. Biol. 114*, 37–45.

Powers, R., Gronenborn, A. M., Clore, G. M., & Bax, A. (1991) *J. Magn. Reson. 94*, 209–213.

Sanders, C. R., II, Tian, G., & Tsai, M.-D. (1989) *Biochemistry 28*, 9028–9043.

Schulz, G. E. (1992) *Faraday Discuss. 93*, 85–93.

Schulz, G. E., Elzinga, M., Marx, F., & Schirmer, R. H. (1974) *Nature (London) 250*, 120–123.

Shaka, A. J., Lee, C. J., & Pines, A. (1988) *J. Magn. Reson. 77*, 274–293.

Shi, Z., Byeon, I.-J. L., Jiang, R.-T., & Tsai, M.-D. (1993) *Biochemistry 32*, 6450–6458.

Spera, S., & Bax, A. (1991) *J. Am. Chem. Soc. 113*, 5490–5492.

Stockman, B. J., Nirmala, N. R., Wagner, G., Delcamp, T. J., DeYarman, M. T., & Freisheim, J. H. (1992) *Biochemistry 31*, 218–229.

Tian, G., Sanders, C. R., II, Kishi, F., Nakazawa, A., & Tsai, M.-D. (1988) *Biochemistry 27*, 5544–5552.

Tomasselli, A. G., & Noda, L. H. (1980) *Eur. J. Biochem. 103*, 481–491.

Tsai, M.-D., & Yan, Y. (1991) *Biochemistry 30*, 6806–6818.

Vetter, I. R., Reinstein, J., & Rösch, P. (1990) *Biochemistry 29*, 7459–7467.

Vetter, I. R., Konrad M., & Rösch, P. (1991) *Biochemistry 30*, 4137–4142.

Zuiderweg, E. R. P. (1990) *J. Magn. Reson. 86*, 346–357.